

Integrated Data Analysis and Dynamic Fracture Modeling Key To Understanding Complex Waterfloods: Case Study of the Pierce Field, North Sea

B. Hustedt, SPE, Brunei Shell Petroleum, and J.R. Snippe, SPE, Shell U.K. Limited

Summary

The performance of many waterfloods [and enhanced-oil-recovery (EOR) schemes] is characterized by fluid injection under fracturing conditions. Especially when the geology is complex and the mobility of the reservoir is low, induced fractures can be of the same order as the well spacing, which has a significant (in general undesired) impact on both areal sweep and vertical conformance. Therefore, fluid injection needs to be actively managed and surveyed in order to design an appropriate injection strategy over time.

We have analyzed historical injection/production-test, injection step-rate-test, and falloff (FO) test (FOT) data of an existing complex waterflood in the Pierce field, North Sea. The mental subsurface model that emerged from this data analysis was developed further through a series of dynamic fracture-propagation simulations. While the data analysis was a relatively standard procedure, the fracture-modeling part was far from trivial and included simulations using a standalone fracture modeling tool and a more sophisticated coupled dynamic fracture-propagation reservoir simulator, both being in-house software tools.

The combined analysis was used to develop a better understanding of the waterflood performance. The main improvement compared to previous work was the integration of the data analysis and the dynamic modeling work rather than looking at each data source individually. In combination, a consistent explanation of the observed reservoir behavior was achieved. This has resulted in changes in the day-to-day water injection management and is expected to play a key role in longer-term development strategies

Introduction

The field geometry is characterized by two salt diapirs that penetrate the reservoir formation, leading to two connected accumulations (North Pierce and South Pierce). Geologically, Pierce consists of many turbiditic sand/shale sequences and only large geological features such as faults are well localized on seismic data.

Since 1999, the field has been developed under depletion drive with gas reinjection. In 2004, water injection was introduced in South Pierce with the dual objective to give additional pressure support and better sweep downdip of the oil producers. The water-injection project consists of a series of highly deviated (horizontal) injector/producer pairs surrounding the South Pierce salt diapir. Each well pair covers approximately one-quarter of the total South Pierce reservoir area (see Fig. 1). Initially, the continuous functioning without operational interruption of the water-injection facilities was poor (complicating the data analysis), which was resolved toward the end of 2006.

Overall, the waterflood response is considered to be effective in terms of increasing the reservoir pressure, while the impact of water injection on areal sweep is problematic. After the start of water injection, initially indications of increasing field rates were recognized. But in the first half of 2006, the producer Well A1

on the east flank of the salt diapir watered out very quickly and unexpectedly. One possible explanation is an induced fracture that created a shortcut from the injector to the producer. Note that the shortest lateral distance between Producer A1 and Injector A8z is on the order of 850 ft (with similar vertical offset). For the two well pairs in the south and west, water cut was increasing somewhat faster than expected (but still much slower than for A1) and, therefore, the water-injection rate was decreased recently. So far, the apparent effect is positive though the time frame is too short to have a reliable explanation.

Optimal water-injection rates are a subtle balance between voidage, induced-fracture growth, and reservoir heterogeneity, and, therefore, each of the injector/producer well pairs requires a detailed data/modeling effort to design an appropriate injection-management scheme.

Waterflood surveillance in Pierce is difficult because of the way the wells have been completed. But it is absolutely essential to provide the basis for the type of analysis that is demonstrated here. Therefore, increasing the understanding of the waterflood response and optimizing the water injection in Pierce rely on the combination of surveillance-data analysis and forward modeling.

In this paper, we demonstrate the analysis that was undertaken to better understand the waterflood using one of the four injector/producer pairs (Specifically Producer A1 and Injector A8z on the east side of the salt diapir).

Combined Approach

In order to improve the performance of the existing waterflood, it was decided to re-evaluate all available field data in an integrated fashion. In the past, mainly injected volumes and tubinghead pressures (THPs) were analyzed in isolation and, therefore, the waterflood behavior was not well understood.

In the current study, the waterflood behavior was analyzed by interpretation of daily injection and production volumes, THPs in injectors and bottomhole pressures (BHPs) in producers (real-time data), FOT analysis using a range of different interpretation models (static fracture and injection-falloff models), and in-house reservoir- and dynamic fracture-modeling tools of varying degrees of sophistication (PWRI-FRAC™ and FRAC-IT™).

The main emphasis of this study is the integrated approach to address the key uncertainties. Consistency between various modeling technologies and data interpretations largely increased the confidence in the results of the study and has led to better understanding of the waterflood response. The re-active waterflood control that was executed during the past years is being replaced by a proactive waterflood management based on and supported by the data-analysis effort.

Raw-Data Analysis

The first step toward a better understanding of the Pierce waterflood response was a detailed analysis of all the raw data available such as daily injection/production rates and THP/BHP, step-rate injection test(s), buildup and FOT in producers and injectors, respectively. In the following, we are presenting an example of each of these data groups, while the stress data and pressure-transient data are discussed in separate paragraphs that follow.

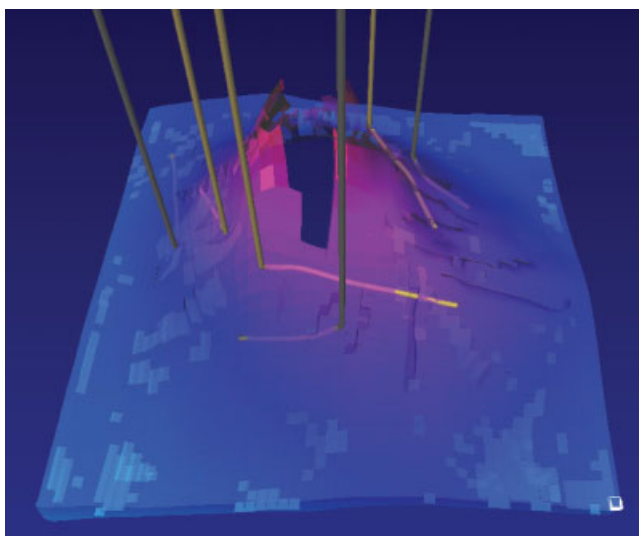


Fig. 1—Water-injector/oil-producer pairs in South Pierce.

Fig. 2 gives an example of injection/production response in Injector A8z and Producer A1 over a time period of 3 months. When Injection Well A8z is closed in for operational reasons, we observe a very quick response (1 or 2 days) in the BHP in A1 (i.e., the BHP starts dropping). On the other hand, as soon as the injection rate in A8z is resumed, the BHP in Producer A1 starts increasing again. This behavior clearly demonstrates the communication between the two wells.

The second data set that we analyzed was an injection step-rate test that was performed in Injector A8z during the startup of the well. In Fig. 3, we plot the injection rate and the THP measured on the rig floor during the test. From the pressure behavior, we estimate a fracture-initiation pressure of approximately 3,100 psi. In Fig. 4, we have plotted THP vs. injection rate. The plot confirms the previously estimated fracture-initiation pressure at approximately 3,100 psi (see change of slope). The step-rate test shows clear indications of the initiation of an induced fracture in the highly deviated injector well. Because of operational reasons, a re-entry in the injector well is not possible and, therefore, a further quantification with additional field data, such as running a production-logging tool (PLT) to see at which point along

the deviated section the fracture initiated, was not feasible. Most likely, induced fractures in highly deviated or horizontal wells initiate at the top of the perforations close to the heel of the well because of two reasons: (i) The heel is the weakest point of the well, and (ii) It is the shallowest point of the well covered with perforations, which under normal conditions has the lowest minimum horizontal stress.

Stress Data

One of the key parameters that influence the performance of water injection is the minimum-horizontal-stress magnitude and stress-field orientation. Given the complex reservoir geometry, with reservoir layers tilting up to 80° toward the salt diapir, only approximate stress-field estimates were feasible.

The stress-field magnitude was estimated using a simple rule of thumb, leakoff tests (LOTs) and formation-integrity tests (FITs) performed during drilling of the appraisal and development wells, and fracture-propagation-pressure (FPP) and fracture-closure-pressure (FCP) estimates recorded during the step-rate and FOT in the injector well. The stress-field orientation was determined by analyzing borehole breakout data and from numerical stress-field computations using a complex finite-element code. Note that the latter study was quite extensive and will be discussed in a future paper.

The rule of thumb used to estimate the stress-field magnitude simply assumes a homogeneous body extending from the sea bottom to the top of the reservoir. We used a minimum-horizontal-stress gradient of 0.8 psi/ft to compute the minimum horizontal stress at the reservoir depth.

The computed minimum-horizontal-stress data were corrected for pressure depletion (approximately 1,800 psi) caused by the production from the Forties reservoir. The minimum-horizontal-stress decrease related to the depletion is estimated using the poroelastic constant ($A_p = 0.66$): $A_p \cdot dP = dS_3$. Note that dP denotes the change in pressure and dS_3 the resulting change in minimum horizontal stress. The complete data set is plotted in Fig. 5.

Borehole breakout data were recorded from three-armed caliper logs in the vertical appraisal wells that are surrounding the salt diapir. The interpretation of the data gives a radial stress-field orientation around the salt diapir. That is, the minimum horizontal stress is tangent to a circle around the salt, and the maximum horizontal stress is pointing toward/away from the salt diapir. Therefore, fracture propagation under the given well configuration would not be favorable in that an induced fracture would grow directly from the injector toward the producer well.

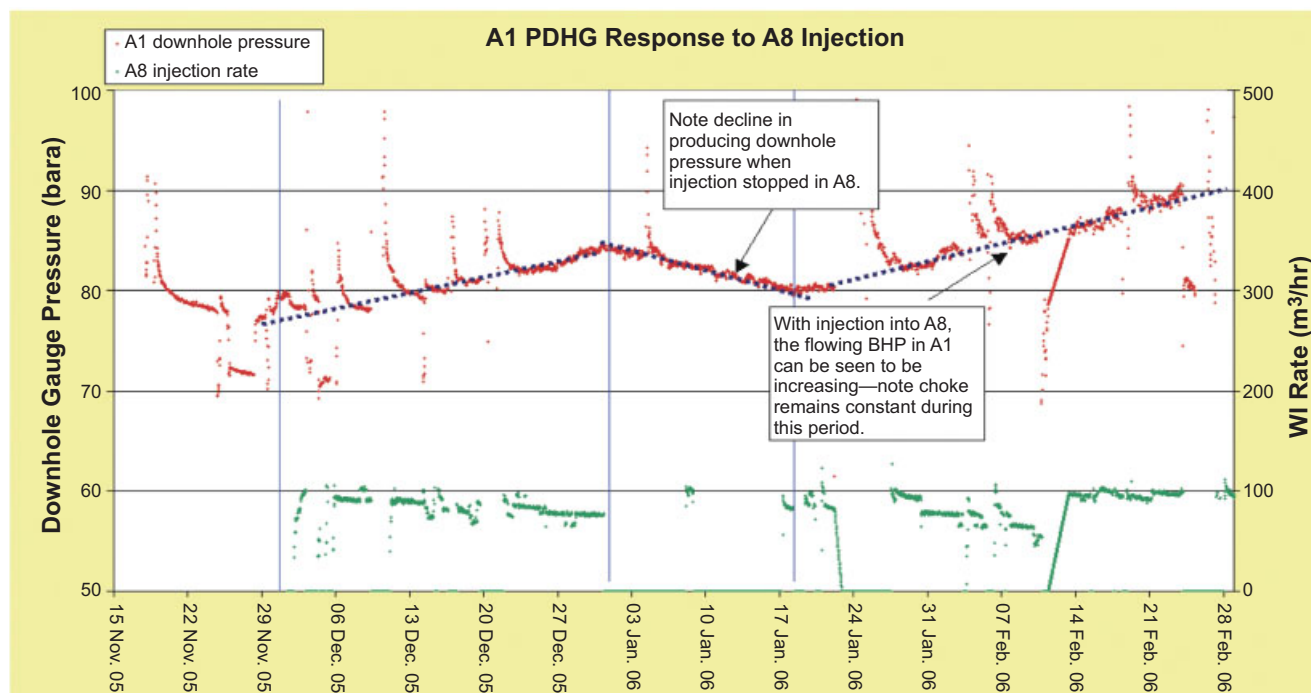


Fig. 2—Injection rate (A8z) and producer (A1) BHP over time.

Pierce A8z—Surface Pressure and Injection Rates while Fracturing

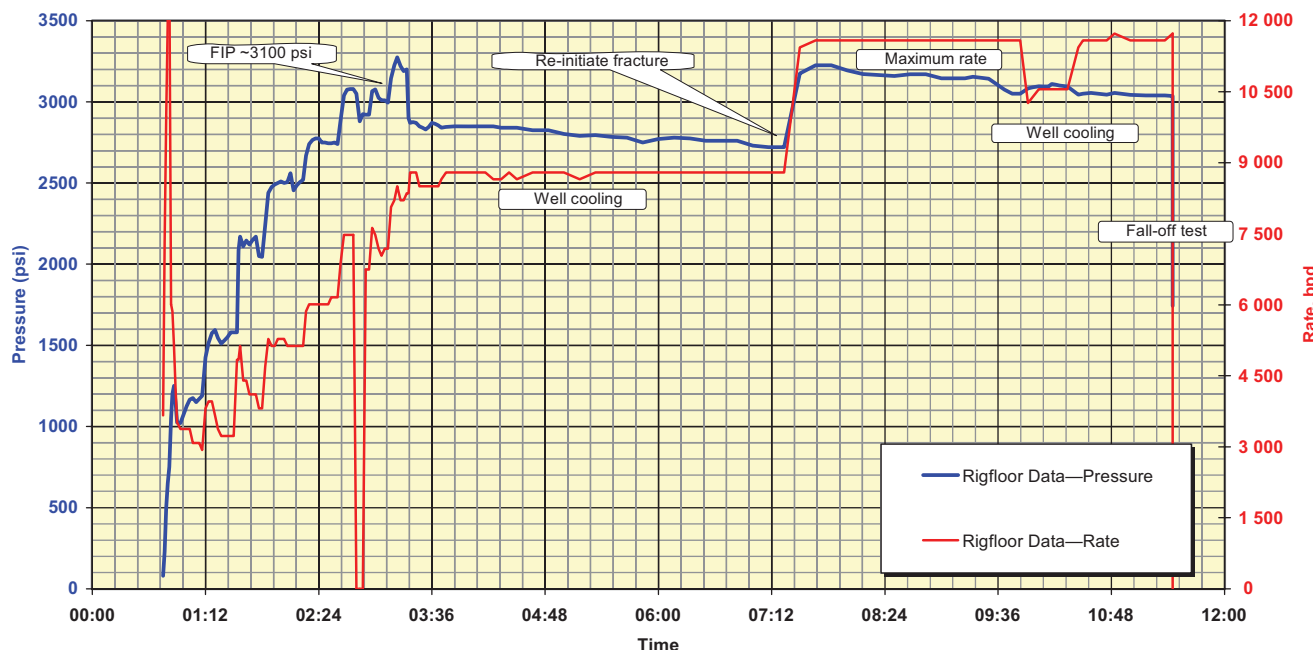


Fig. 3—Step-rate injection test in Injector A8z.

The local stress field might be much more complex because of major approximately radial faults surrounding the salt diapir and because of differential depletion and reservoir heterogeneity. Given the available data, we were not able to obtain a better stress-field estimate at the time of this study and, therefore, used the data from Fig. 5 throughout this study. Also, stress contrasts with the overlying shales and underlying degrading reservoir rocks were unknown and, therefore, treated as an uncertainty during the study.

Well-Test Interpretation

We analyzed a series of well tests (step-rate and FOT) that occurred from start of water injection in A8z until June 2008. Because of

operational constraints in Pierce, we were not able to design a dedicated FOT that would increase the chances to estimate accurately (e.g., the fracture dimensions). Therefore, we selected one step-rate test that was performed during the startup of Water Injector Well A8z and two shut-in periods called FO#101 and FO#237. During the shut-in periods Injector A8z was shut in for operational reasons. No special shut-in procedures were put into place, and data-sampling rates were relatively modest (somewhat better for FO#237 than for FO#101, down to 1 minute). In Fig. 6, we show the whole set of injection data loaded into Saphir™ for the period from December 2005 until April 2008. Highlighted in blue are the two aforementioned FOTs. We have selected two FOTs in order to

A8z Injection Test

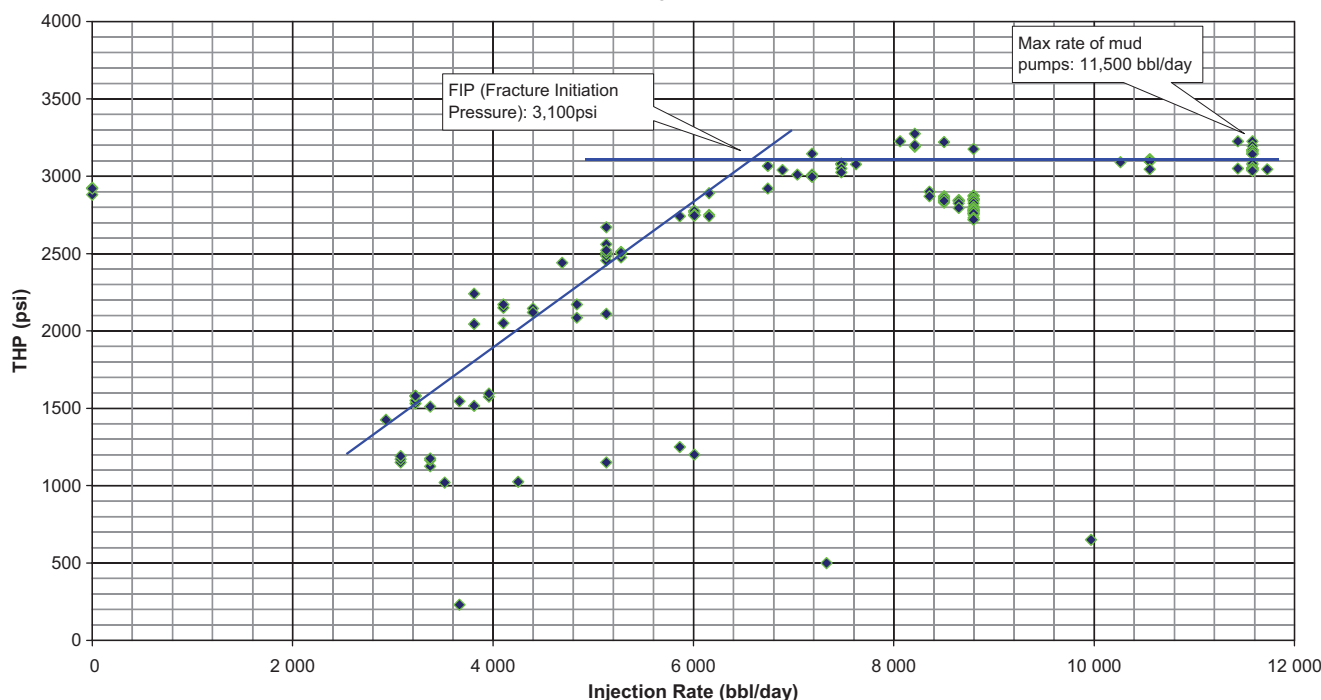


Fig. 4—THP vs. injection rate (green dots) during step-rate injection test in Injector A8z. Note that the two blue lines indicate matrix and fracture injection regimes. The interpreted fracture-initiation pressure is 3,100 psi.

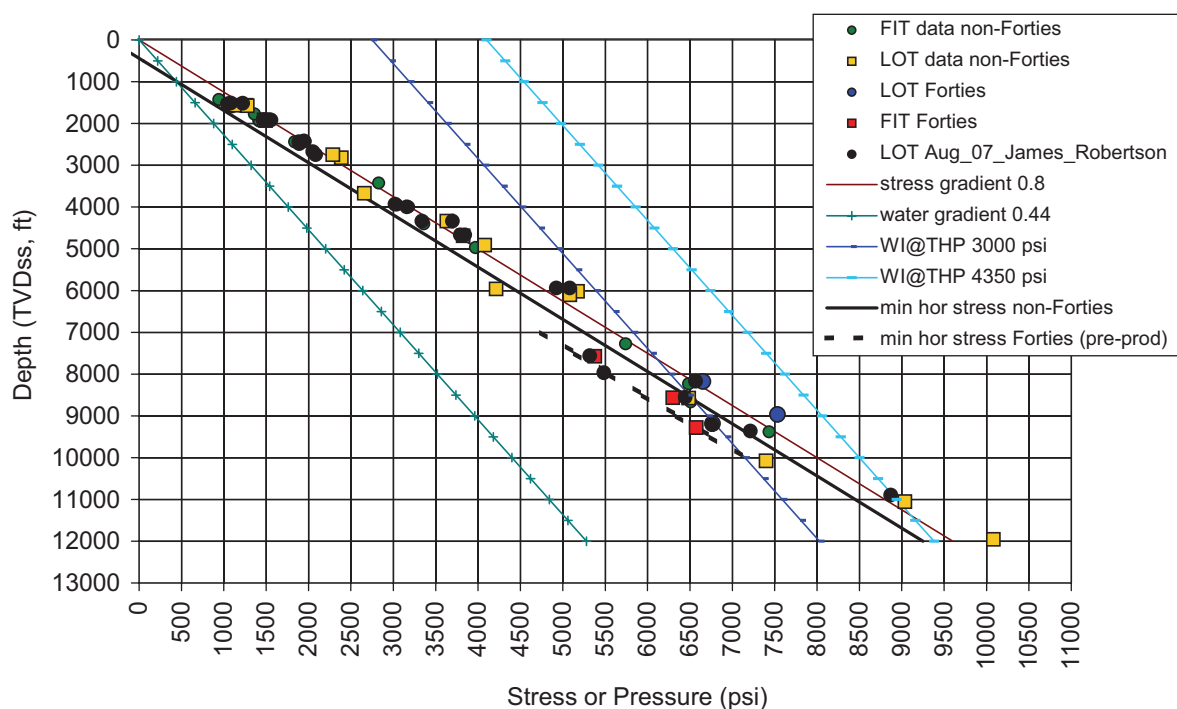


Fig. 5—Stress data used for estimating minimum horizontal stress.

see the development of a potential fracture over time. FOs #101 and #237 correspond to injection times of 135 (May 2006) and 615 (January 2008) days.

For the SRT interpretation we used a standalone dynamic fracture-propagation simulator (called PWRI-FRAC™) to verify the learnings from the pure data analysis and estimate initial fracturing parameters such as FPP and initial fracture dimensions. The

simulator calculates dynamic fracture dimensions and bottomhole injection pressures over time resulting from the injection of seawater or produced water. The reservoir model is described by a set of parameters that are defined on a layer-per-layer basis (e.g., Young's modulus, Poisson's ratio, permeability, porosity). Note that reservoir layers are infinite in extent. The main model parameters for one simulation example are given in **Table 1**.

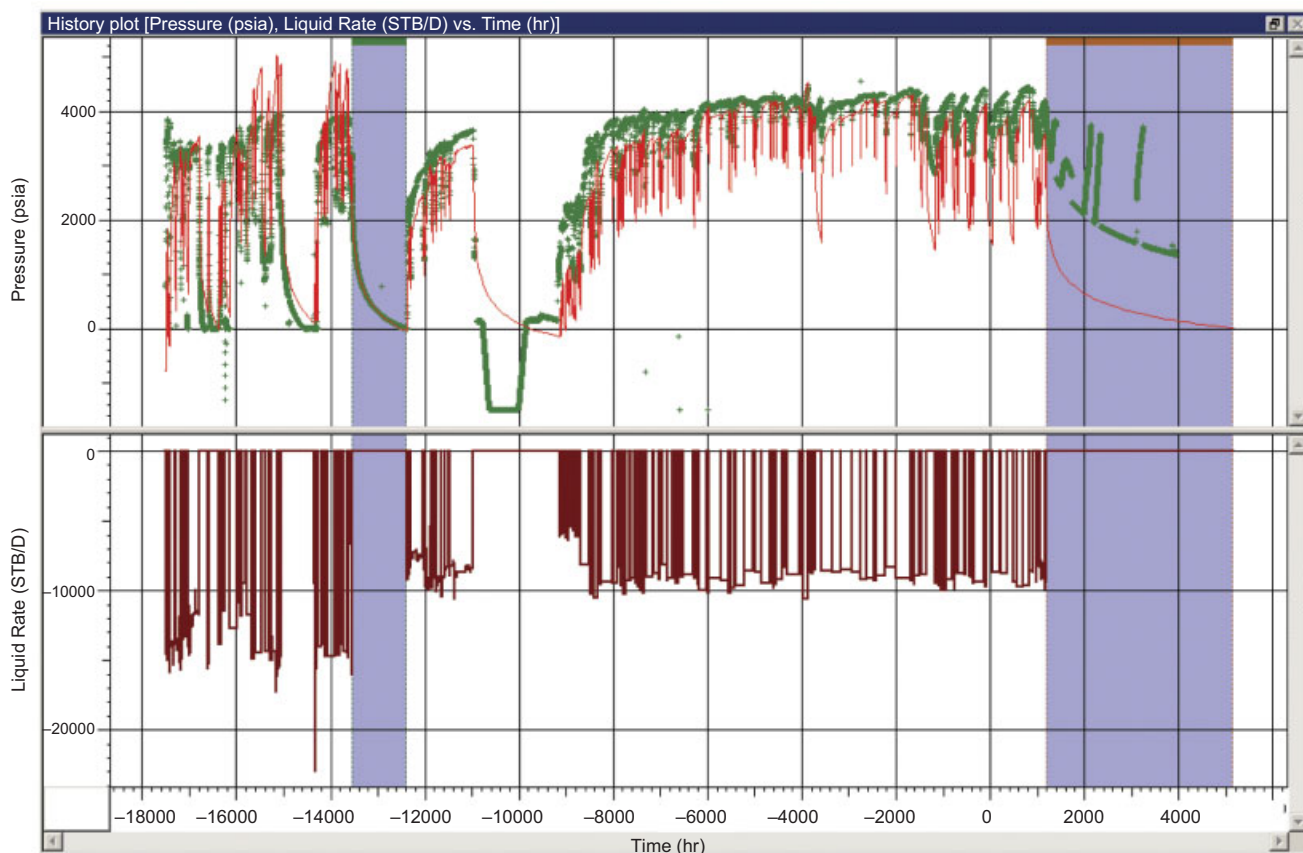


Fig. 6—Injection data from December 2005 to April 2008. FOTs (#101, #237) are highlighted in blue.

TABLE 1—EXAMPLE OF PWRI-FRAC INPUT PARAMETERS

Stress gradient, psi/ft	0.8	Poroelastic constant	0.66
Pressure gradient, psi/ft	0.44	Thermoelastic constant, psi/°F	8
Permeability, md	15	Reservoir temperature, °F	230
Porosity	0.18	Total reservoir compressibility, 1/psi	6.9 E-6
Young's modulus, GPa	8	Water viscosity at T_{inj} , cp	0.29
Poisson's ratio	0.2	Water viscosity at T_{res} , cp	1.26
Net to gross	0.6		

For the FO analysis, we have used two different models. At first, we used a static fracture model with infinite conductivity, which implies that the fracture stays open (is static) even after closure of the well. This is not entirely correct because it is well known that induced fractures shrink and/or close after shut-in of the well. The degree of closure, or how much of a flowpath remains open after fracture closure, is not known, but in many cases the response of the pressure decline is not characteristic of or comparable to the response of a static fracture. On Pierce, however, the mid- to late-time response is likely to be similar because matrix permeabilities are relatively low (≈ 15 md) such that on a relative scale the residual fracture permeability is very likely to be large. Note that we refer to the infinite-conductivity static fracture model as ICSF in the following.

The other model has been designed especially to interpret FOTs from water-injection wells and is called the injection-falloff (IFO) model (van den Hoek 2005). The IFO model incorporates a pressure-dependent storage contribution that accounts for the closing-fracture effect on the pressure decline. From the pressure decline, IFO estimates fracture dimensions (fracture half-length and fracture height upward and downward), dimensionless fracture conductivity, and potential noncontainment in the injection layer.

For all FOT interpretations, we assumed a fault that influences the mid- and late-time data. From seismic data, we know that there are large faults in this area, and from a repeat formation tester (RFT) run before production in Producer A1, we know that A1 intersects a "feature" that is sealing or at least baffling.

SRT Interpretation. The best THP match of the SRT obtained with the dynamic fracture simulator is shown in Fig. 7. In order to achieve the match, we introduced a shale layer below the

fracture-initiation point such that the injection-layer thickness is constrained to 60 ft instead of the total layer height of approximately 200 ft. The resulting best-match fracture dimensions are 30-ft fracture half-length, and 21-ft and 27-ft fracture height upward and downward, respectively. Therefore, the fracture was contained in the injection zone. Note that we used a positive stress to the overlying shale layer because of the depletion-related stress reduction in the injection layer (see the Stress Data section). At low injection rates we are not able to match the data because injection is most likely still under matrix conditions. For higher injection rates, the obtained match fits the measured THP very well.

From the start of water injection in December 2005 until January 2008 the reservoir pressure (as measured at Producer A1) increased by approximately 70 bar. Because the standalone fracture simulator does not capture reservoir-pressure changes over time, we did not consider PWRI-FRAC™ for longer-term history-match simulations.

Overall, the standalone fracture simulations confirm the stress gradient and indicate the effective layer thickness seen by the fracture.

FO #101. We first applied the ICSF model with a homogeneous reservoir to match the FO#101. Fig. 8 shows the best-match result. We observe that the pressure decline and derivative in FO#101 change with a quarter slope from very early times (0.1 hours) until approximately 100 hours. At 100 hours, the derivative starts to flatten out, which we interpret as the onset of radial flow. At approximately 600 hours up to the end of FO #101 at 1,000 hours the derivative bends down slightly. As can be seen from Fig. 8, we were not able to match the latter behavior with this model, but there are many potential explanations unrelated to the induced

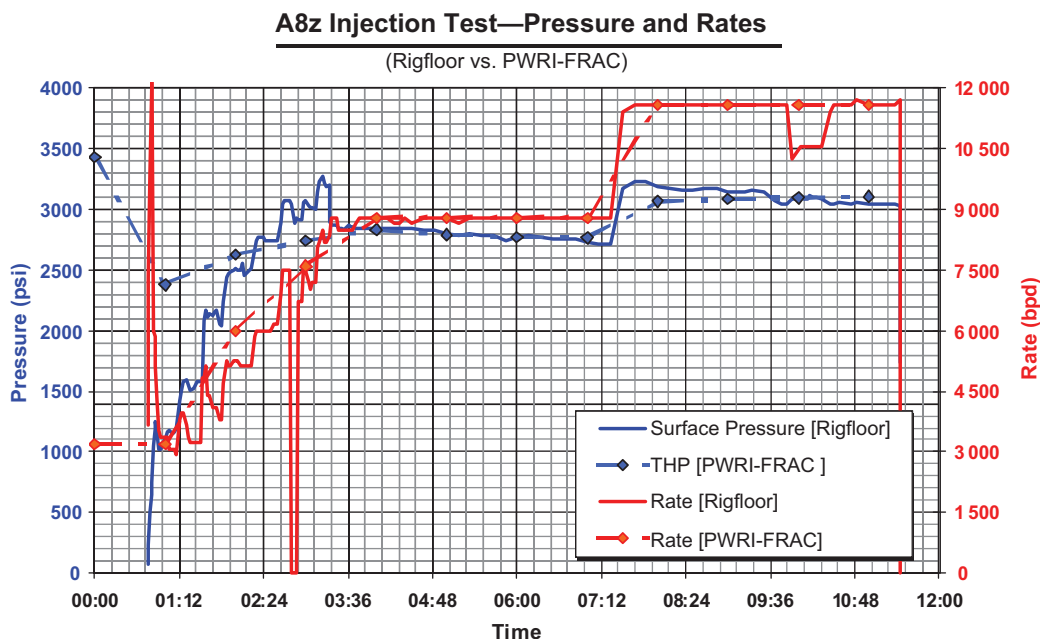


Fig. 7—History-matched injection test in Injector A8z.

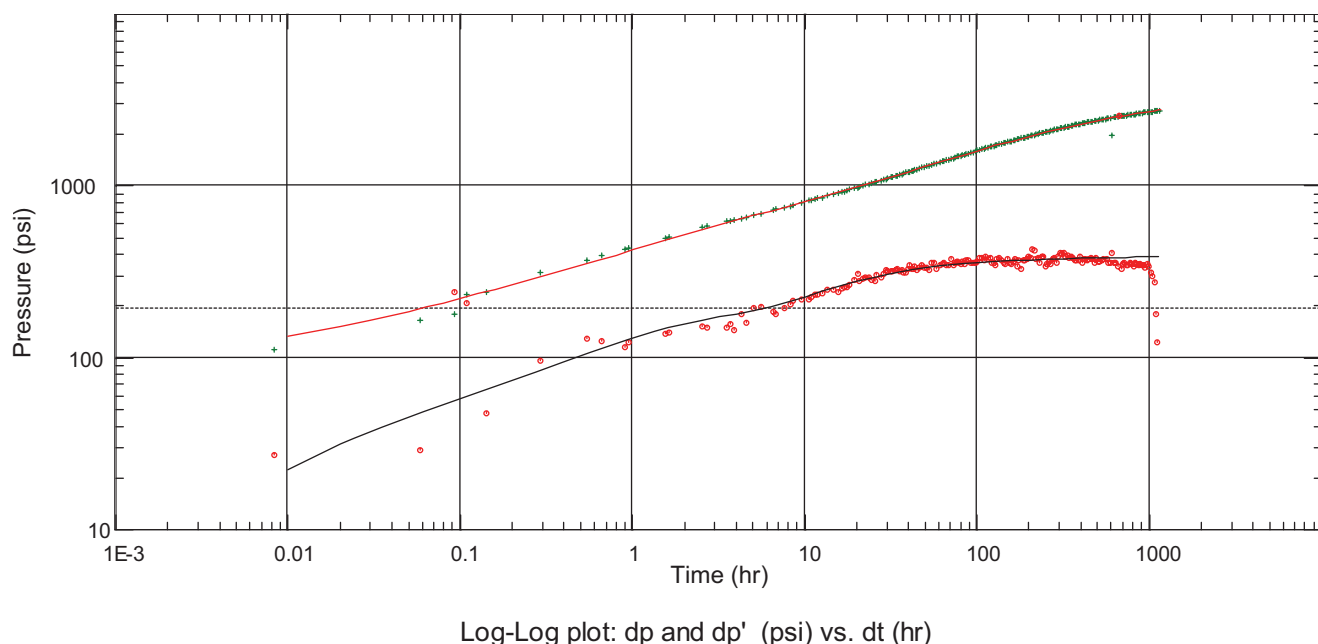


Fig. 8—FO #101 interpretation with the infinite-conductivity model. Green crosses and red dots show measured and computed pressure decline (dp) and its derivative (dp'), respectively. The red and black lines show the respective model fits of dp and dp' .

fracture (i.e., later trend in permeability/effective viscosity/layer thickness).

In Fig. 9, we plot the best fit obtained with the IFO model. Overall, the pressure and derivative are matched equally well (neglecting slight differences). As for the ICSF model, we are not able to match the slight drop off in the derivative toward the end of the FOT (> 600 hours). Output parameters for both models are given in Table 2 and are discussed below.

In Fig. 10, we plot the match for FO #101 obtained from either the ICSF model or the IFO model applied for the whole injection

sequence. We observe that the model parameters determined from FO #101 also match the pressure at the beginning of the injection. After the first small shut-in periods, the match significantly degrades in that computed pressures largely exceed the measured pressures. This implies that a dynamically growing fracture had been larger during these periods of time. From FO #101 until the end of the injection, we note that the matched THP is a bit too low and that FO #237 is not matched at all. In this period, the pressures during shut-ins are too low while the pressures during injection are too high. This suggests on the one hand an increase

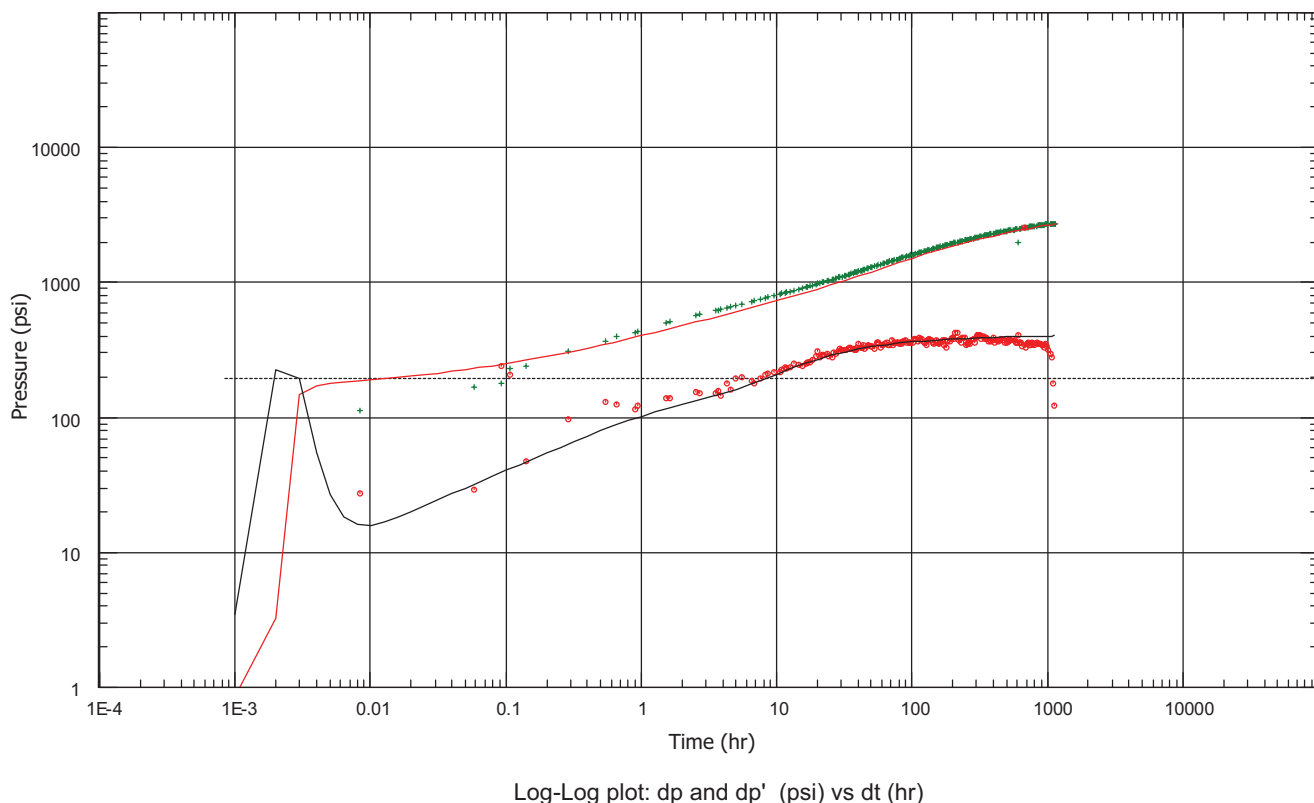


Fig. 9—FO #101 interpretation with the IFO model. Green crosses and red dots show measured and computed pressure decline (dp) and its derivative (dp'), respectively. The red and black lines show the respective model fits of dp and dp' .

TABLE 2—RESULTS FROM FOT ANALYSIS

	FO#101		FO#237	
	ICSF	IFO	ICSF	IFO
kh, mdft	610	610	410	410
Xf, ft	141	220	660	700
L, ft	396	400	912	900
h, ft	54	54	54	54
hf, ft	54	—	54	—
hf1, ft	—	50	—	30
hf2, ft	—	50	—	25
Skin	0.233	—	0.105	—
C, bbl/psi	1 E-3	—	1 E-3	—
Fskin	—	0.4	—	0
FcD	—	10,000	—	1,000

in reservoir pressure over time that is not captured by the interpretation (not unexpected since the interpretation assumes an open system, namely, only a single fault), and on the other hand, again, an increase in injectivity (dynamically growing fracture).

FO #237. We apply the ICSF model and the IFO model to match the FO at the end of the injection sequence. Fig. 11 shows the best fit that was obtained with the ICSF model. Note that the last FO (#237) is related to operational constraints and has not been designed/executed to obtain the best possible data for this analysis. As a result, we observe numerous pressure disturbances after 40 hours of shut-in time. These are related to operational interferences. Since the reason for the disturbances is known, the spurious time periods can be filtered out. After this filtering, the trend of the pressure decline is clearly visible, and, therefore, we decided to use the test for the analysis.

FO #237 is characterized by an almost quarter slope (slightly less) that extends from the start of the test until approximately 600 hours after shut-in. Note that the early-time data (< 10 hours) shows much more scatter compared to FO #101 (which is simply because of the higher sampling rate). At shut-in times longer than 600 hours, the pressure derivative starts to flatten out, which we interpret as the onset of the radial-flow regime.

The IFO match for FO #237 is shown in Fig. 12. Compared to the ICSF match in Fig. 11, the IFO interpretation for the pressure and pressure derivative in Fig. 12 gives a poorer match. We would like to stress though that the IFO match delivers a reasonable fit to the data with similar matching parameters [i.e., fracture half-length (X_f)], thus (given the better representation of the physics in IFO than in ICSF) adding to the confidence that the X_f extracted from ICSF is reasonable. Output parameters for both models are given in Table 2 and are discussed below.

Discussion. The two FOTs (#101 and #237) show similar behavior in that the pressure difference and its derivative increase with a quarter slope on a log/log plot over a long period of time. At approximately 100 and 600 hours, the derivative is flattening out and we observe radial flow for FO #101 and FO #237, respectively. The increase in time until radial flow is observed is because of a change in fracture dimensions (vertical fracture shrinkage and horizontal fracture growth).

In addition to the fracture half-length that is obtained also with the ICSF model, the IFO model also provides insights as to whether or not the induced fracture before the shut-in was contained in the injection zone and whether a stress contrast to the over- or underlying shale layers was present. Type curves for the pressure decline observed during an FOT with a closing induced fracture present have been shown and discussed by van den Hoek (2005). In Fig. 13, we show type curves for fracture length vs. height shrinkage as presented by van den Hoek (2005). Figs. 13a and 13b show the dimensionless pressure decline and its derivative, respectively, for

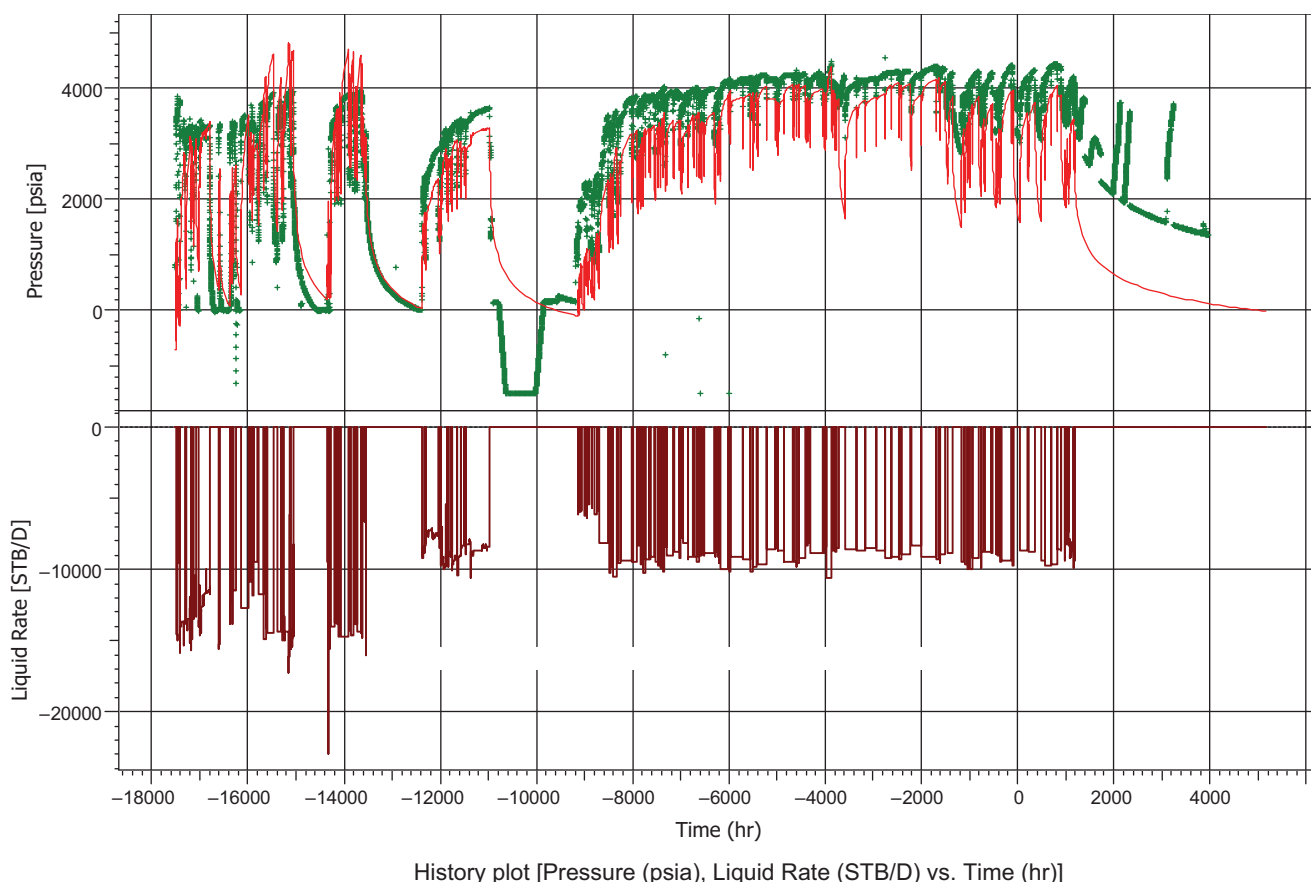


Fig. 10—FO #101 match applied to full injection sequence. Green crosses show the measured pressure data and the red line the respective model response over time.

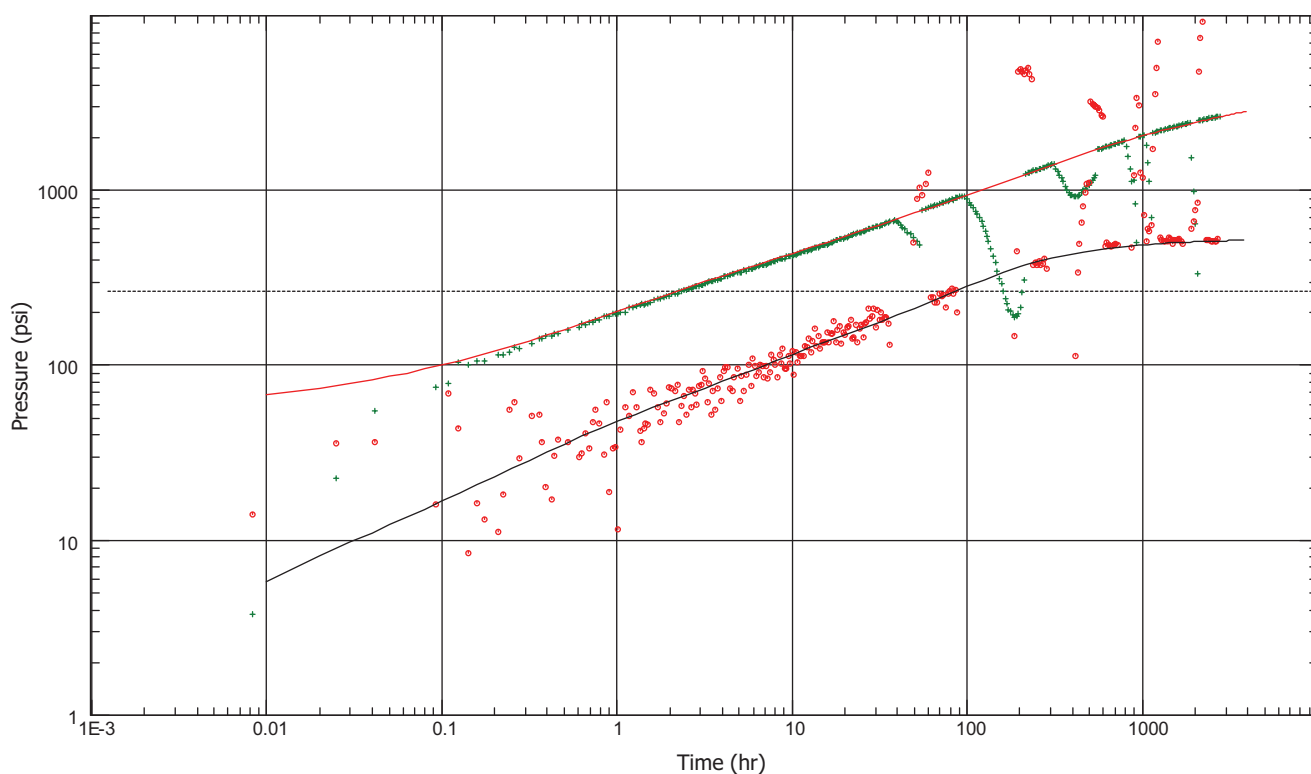
Log-Log plot: dp and dp' (psi) vs. dt (hr)

Fig. 11—FO #237 interpretation with the infinite-conductivity model. Green crosses and red dots show measured and computed pressure decline (dp) and its derivative (dp'), respectively. The red and black lines show the respective model fits of dp and dp' . (color)

an induced-fracture closure that is characteristic for length and height closure. From this work, we conclude that the pressure decline observed in A8z is characteristic of a long and elongated fracture that is contained in the injection zone. This conclusion is

driven mainly by the fact that the response from the early-time data is slowly increasing without any major disturbance similar to the ones presented by van den Hoek (2005) for a vertically non-contained fracture (large peaks in the early-time data on log/log plot).

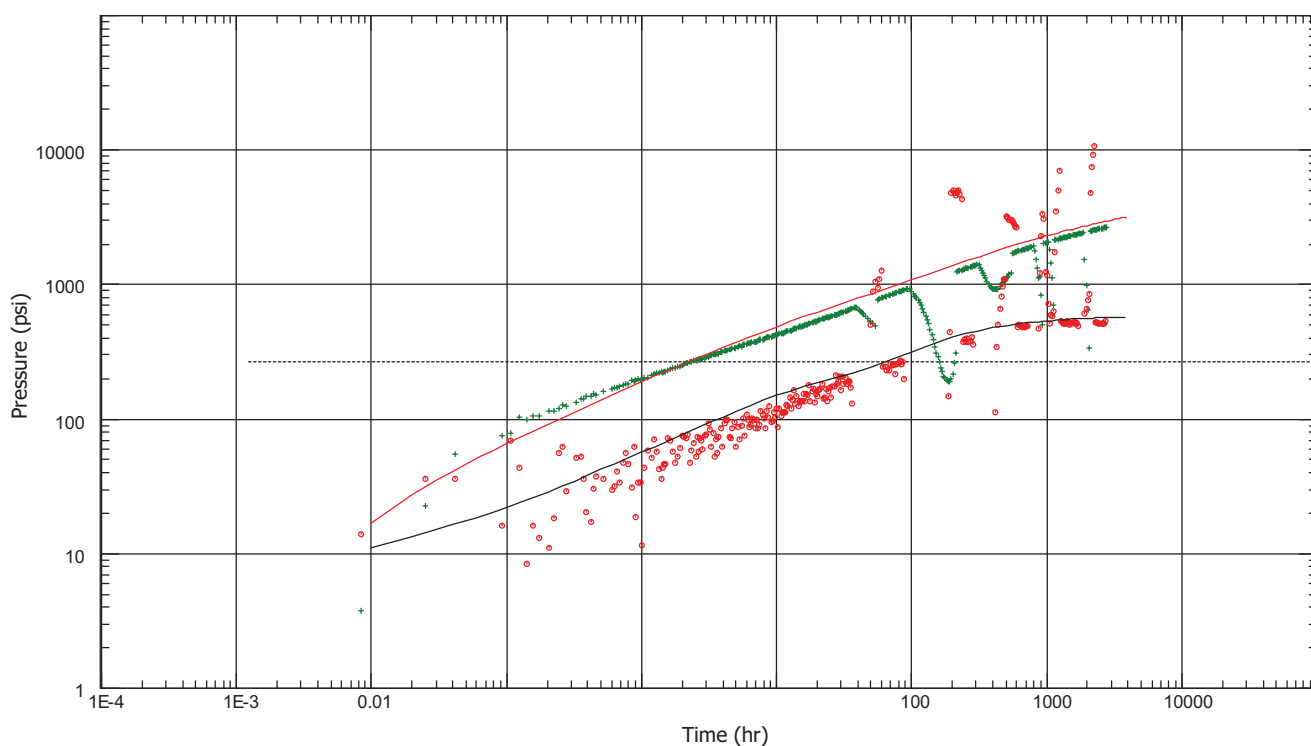
Log-Log plot: dp and dp' (psi) vs. dt (hr)

Fig. 12—FO #237 interpretation with the IFO model. Green crosses and red dots show measured and computed pressure decline (dp) and its derivative (dp'), respectively. The red and black lines show the respective model fits of dp and dp' .

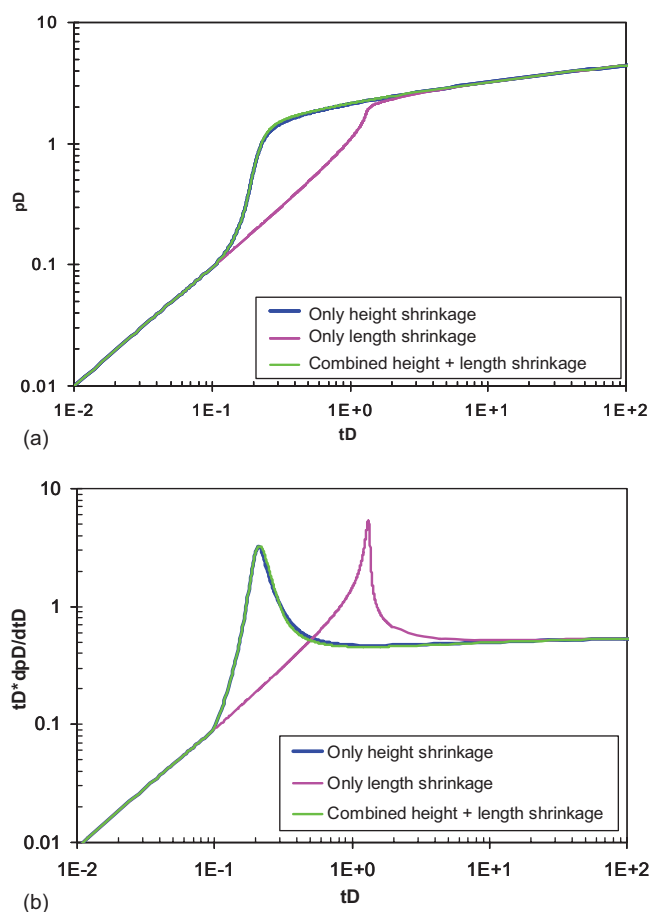


Fig. 13—Type curves for fracture-length vs. -height shrinkage as presented by van den Hoek (2005).

Note that pressure data at very early times and at a high sampling frequency are not available (because of operational constraints), and, therefore, a potential clear fracture-closure signature as described by van den Hoek (2005) might not have been captured. Still, the absence of these characteristics points toward an induced fracture that has been propagating mainly in the length direction. Also, when increasing the fracture-height dimensions beyond the best-fit total fracture height ($hf1 + hf2 > hf1^{bf} + hf2^{bf}$, where bf means best fit or contained) and varying other fracture parameters (such as fracture half-length), we were not able to obtain a reasonable fit of the falloff data. This further supports the conclusion that the induced fracture is most likely contained in the injection zone.

In Table 2, we summarized the results from both the ICSF-model and the IFO-model interpretations. Note that the kh and distance to the fault were kept fixed deliberately for interpretations of a given FO in order to ensure comparable results.

We observe that for FO #101, the ICSF-model interpretation results in a smaller fracture half-length than the IFO interpretation (220 ft). Moreover, IFO requires a fracture that has been growing in height out of the injection layer. The injection-layer height used in the model is 54 ft, and IFO requires a total fracture height ($hf1 + hf2$) of approximately 100 ft with hardly any stress contrast between the injection zone and the over- and underlying formations. Note that the total reservoir thickness in this area is estimated to be approximately 200 ft, so one could speculate that the fracture connects to a 100-ft-thick sand/shale package (i.e., half the reservoir) with an average net to gross of approximately 50 to 60%.

As we already mentioned, the match of FO #101 plotted over the whole injection cycle indicates that before FO #101, that is in the first half of 2006, an induced fracture with greater dimensions was present.

The results of the IFO interpretation of FO #237 (May 2008) give a fracture that is now contained within the injection zone.

This implies that the fracture has been shrinking vertically between June 2006 and May 2008. For the same time, IFO now predicts a fracture half-length of approximately 700 ft. The ICSF-model interpretation results in fracture dimensions that are very similar to the ones obtained with the IFO model (i.e., a fracture half-length of approximately 660 ft).

The heterogeneity of the geology and the seismic shadow zones caused by the salt diapirs in Pierce only allow very conceptual subsurface models that can explain the described data. Models that fit all observed and interpreted data require some sort of permeability heterogeneity (high-permeability reservoir streak) that was connected by an induced fracture during periods of time (fracture-height growth and shrinkage). The one parameter that can be determined unambiguously (from radial flow) is the permeability-height product (kh). Therefore the permeability (k) is a free-scaling parameter that can potentially be used to derive a consistent set of model parameters (e.g., distance to the Fault L) that fit the discussed FO behaviors.

Overall, for a given FO the agreement between the ICSF and IFO models is very satisfactory. The combined analysis and interpretation from an induced-fracture perspective helped to develop a conceptual subsurface model that can explain all of the measured data. Of course, there are differences that remain and parts that are not yet fully understood.

FRAC-IT

We apply the coupled simulator [FRAC-IT™ (Hustedt et al. 2005)] to address the shortcomings of the standalone fracture simulations. The FRAC-IT™ simulations are used to provide a pressure history match and fracture dimensions over time such that horizontal fracture growth, vertical fracture containment, and potentially swept reservoir areas (where does the water go?) can be estimated or identified.

As was described by Hustedt et al. (2005, 2008) and van den Hoek et al. (2008), the FRAC-IT™ simulator couples a full-physics reservoir simulator with a dynamic fracture-propagation routine. In contrast to previous coupling approaches, FRAC-IT™ does not require a purpose-built fracture/reservoir model [like REVEAL™ and Tran (2002)], but is a plug-in to a fully history-matched dynamic reservoir-simulation model.

For the Pierce field, a history-matched full-field model was already available and FRAC-IT™ was added to study the dynamic fracture propagation, as described in the preceding. The properties of the Pierce simulation model away from areas with well control (porosity, permeability, sand-body connectivity) have been populated by means of geostatistical algorithms. These algorithms are applied in the geological modeling tool that forms on a fine-scale the basis of the dynamic simulation model.

For simplicity and to minimize CPU time, we have cut out sector models from the full-field model for each injector/producer pair. Each sector model was defined such that it behaved pressurewise relatively independently from the rest of the field, yet each sector's boundary conditions (pressure) were controlled by the full-field simulation.

In this paper, we demonstrate the data-analysis and modeling approach by selecting the injector (A8z)/producer (A1) pair that is located on the east flank of the salt diapir (see red ellipse in Fig. 1). Note that similar studies have been performed for the remaining well pairs.

The sector model for A8z-A1 incorporates approximately one-quarter of the reservoir area surrounding the salt diapir. As can be seen from Fig. 14, the injector well and the producer well are fully contained in the sector model. We use constant-pressure boundary conditions for the sector model, which is a reasonable approximation over the time scale of the FRAC-IT simulation. We confirmed this by comparing to the full-field-model simulation results. No other alteration to the sector model has been made.

The previously mentioned fault that has been identified in Producer A1 had already been implemented as a sealing fault in the simulation model. All other key model parameters are given in Table 3.

Because of the lack of field measurements, rock properties such as Young's modulus and Poisson's ratio have been estimated

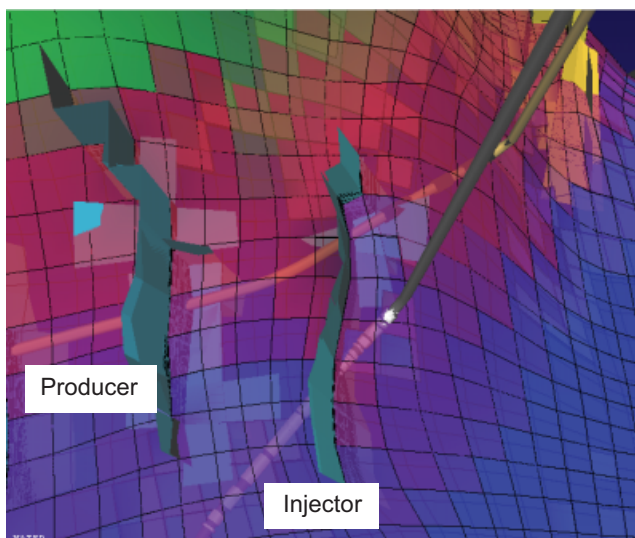


Fig. 14—Part of sector model cut out around Injector A8z and Producer A1.

using data from analog fields. The minimum horizontal stress has been implemented vertically on a gridblock level while laterally the minimum horizontal stress was kept constant.

Fracture initiation is not modeled in FRAC-IT, and, therefore, the user is required to provide an estimate of the initial fracture dimensions and the fracture-initiation point along the wellbore. Since no field data such as a PLT is available to estimate where a dynamic fracture had (potentially) initiated, we have chosen the fracture-initiation point close to the top of the perforations at the heel of the highly deviated Injector Well A8z (see Fig. 15). In general, this is the weakest point of the well and has the lowest minimum horizontal stress. Note that we have simulated sensitivities with respect to other possible fracture-initiation points along the injector well (deeper in the formation), but the resulting pressure response did not fit the observed data.

In order to obtain a history match for the whole injection period from December 2005 to June 2007, we have used monthly averaged injection rates (see orange and blue lines in Fig. 16). Sensitivities have been simulated for a number of input parameters such as water quality (total suspended solids), minimum horizontal stress, poroelastic constant, fracture-initiation point, and initial fracture dimensions.

We have plotted the best match history match in Fig. 16. Note that measured THP is plotted in turquoise, and simulated THP and BHP are in pink and brown, respectively. Computed fracture dimensions are given with respect to the center of the symmetric fracture (ellipse) as fracture half-length (purple), fracture height upward (grey), and fracture height downward (green).

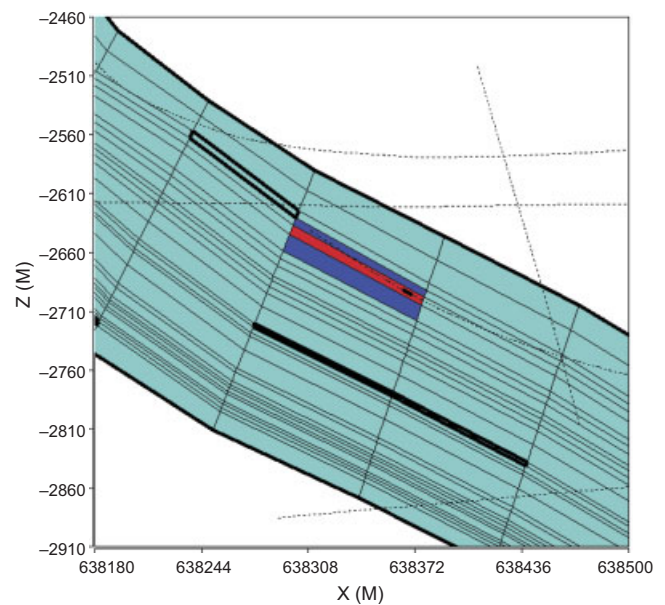


Fig. 15—Cross section through sector model at start of fracture propagation. Red and blue colors denote the gridblocks that are connected by the fracture.

Since no BHP data are available we have concentrated on matching THPs. From Fig. 16, we observe a rather poor match of the THP during the first 4 months of simulation time (until March 2006). This is probably related to the fact that the monthly averaged injection rates do not capture all the small shut-in periods that happened in reality. This results in a rather continuous injection period in the simulation model from December 2005 until June 2006, while in reality many short-lasting shut-in periods occurred. Note that during each shut-in of the injector, most likely an induced fracture closes and needs to be reopened when injection is resumed. The effect of a shut-in period on the computed fracture dimensions can be observed in Fig. 16 during the period May–July 2006 where the fracture half-length decreases by approximately 40%. The small-scale shut-in periods and their resulting effects are not captured in the current history match and can explain the large discrepancy of the matched THPs during the first 6 months of simulation.

Thereafter, from June 2006 to June 2007, a good match of the THP is obtained that captures the overall trend of the pressure behavior. Overall, the application of FRAC-IT™ significantly improves the obtained pressure match in comparison to the PWRI-FRAC™ simulation.

As can be observed from Fig. 16, the induced fracture propagates mainly in the length and downward direction. Upward growth is very limited because the fracture-initiation point is very

TABLE 3—FRAC-IT PRINCIPAL MODEL PARAMETERS

Formation	Sandstone
Depth	9,000 ft
Permeability	approximately 15 md
Water viscosity at injection temperature	1.26 cp
Formation fluid viscosity	0.30 cp
Injection	Horizontal injector/producer pair
TSS	10 ppm
Simulation time	28 months
Number of gridblocks	29×29×33
Injection rate	0–1600 m ³ /day
Young's modulus	8 GPa
Poisson's ratio	0.2

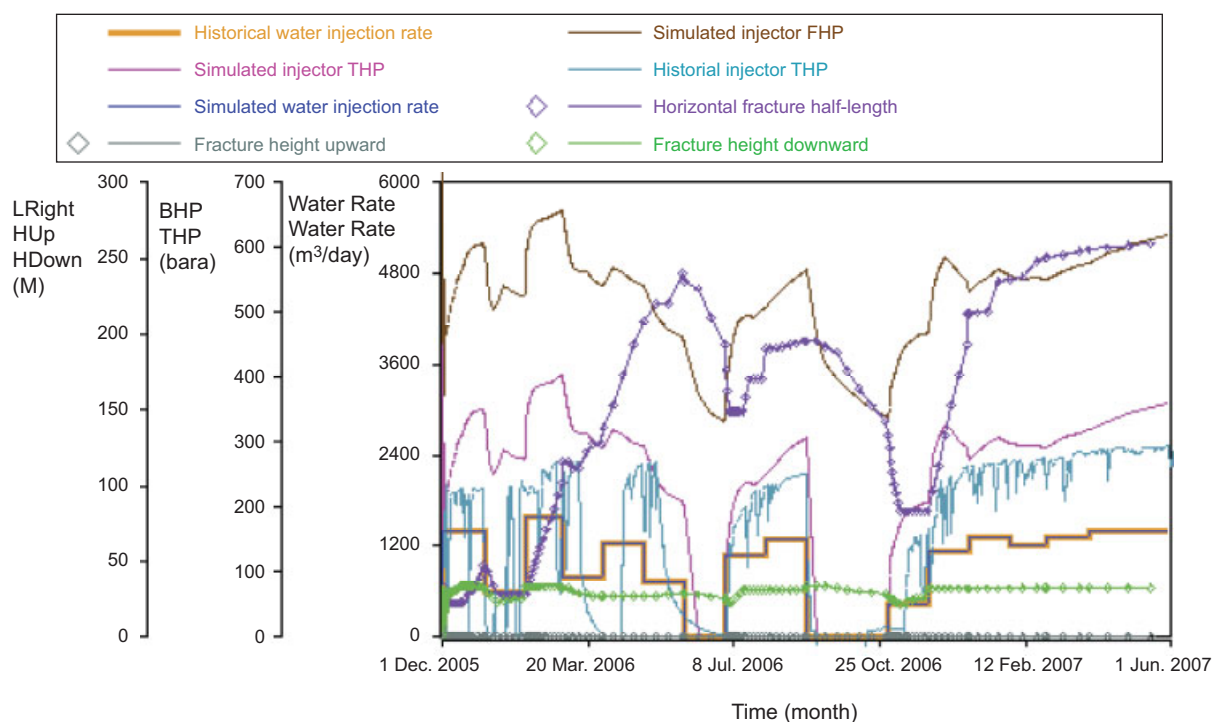


Fig. 16—FRAC-IT history-match simulation results.

close to the upper boundary of the reservoir layer in which the positive stress contrast prevents the fracture from breaking into the overlying shale. Fracture growth downwards is also contained by reservoir heterogeneity at approximately 100 ft. Therefore, the fracture dimensions mainly change in the horizontal direction with varying injection rate.

Three major injection periods have been selected to span the period from December 2005 to June 2007. The first period lasts from the start of water injection until June 2006, the second period from July 2006 to September 2006, and the third period from October 2006 until June 2007. Each of the periods is discussed separately below.

Period of December 2005–July 2006. During the first period, the injection rate in the simulation model varies between 1600 and 700 m³/d. Note that we have neglected the actual short-duration shut-in periods. The computed THP ranges from 300 to 400 bar. As was mentioned in the preceding, the fracture grows in height immediately after start of the water injection until it is contained by the overlying stress contrast and the underlying reservoir heterogeneities. Length growth is initially smaller than height growth. After approximately 1 month of injection, fracture-length growth resumes and starts to increase very rapidly in January/February of 2006, which is directly related to the large increase in injection rate by approximately 1000 m³/d. Even when injection is reduced in March 2006, the fracture propagation continues in the length direction, though at a slower rate, until the shut-in of the well in June 2006. By this time, the fracture has reached a half-length of approximately 800 ft, which is on the order of two-thirds of the injector/producer spacing (approximately 1,200 ft). In the following shut-in period that lasts approximately 1 month, the fracture length reduces to approximately 500 ft. We also observe a very slight shrinkage in fracture height.

Period of July 2006–October 2006. During the second period, the injection rate varies between 1300 and 1100 m³/d, which results in increasing fracture dimensions. The fracture height downwards increases slightly to a height somewhat smaller than during the first injection period. The fracture half-length grows from 470 ft to approximately 630 ft in September 2006. Next Injector Well A8z was shut-in for a period of 2 months in which the fracture

half-length decreased to 220 ft, accompanied by a small decrease in fracture height downwards.

Period of October 2006–September 2007. During the third period, the injection rate varies between 1400 and 1200 m³/d. Now, the maximum injection rate is some 200 m³/d smaller than during the first period and injection-rate variations are within a 200-m³/d range rather than a 1000-m³/d window as in the first period. Overall injection-rate variations are much smaller, and the water-injection uptime is significantly improved, with no further shut-in period between November 2006 and June 2007. As a consequence, the fracture half-length increases rapidly to its previously maximum value of approximately 800 ft and then continues growing slowly until June 2007 to a total fracture half length 850 ft.

Summary. During the 28-month injection period, the dynamic fracture propagates to a total length of approximately 850 ft and fracture height of 100 ft in June 2007. The simulated fracture dimensions in February 2006 and again in June 2007 are on the order of two-thirds of the injector/producer well spacing (1,200 ft), which implies that a dynamic fracture is a reasonable explanation for the fast water breakthrough that was observed in Producer A1. We are confident that the original simulation model at start of water injection is a good base model for the dynamic fracture simulation because the downhole pressure gauge in A1 has a good pressure match but the water breakthrough time in the A1 was not well matched. Though not well matched yet, the FRAC-IT™ simulations bring the water front much closer to A1 at the time A1 had water breakthrough and, therefore, improve the history match significantly. When considering the large reservoir uncertainties (even though the model has been history matched) and that, most likely, real everyday injection rate was never as smooth as shown in Fig. 16 (for example, a short-duration “trip” of very high injection rate), the discrepancy between the simulated fracture dimensions and the geometrical injector/producer distance is negligible. Of course, these small-scale effects that can result in temporary large fractures will never be captured in the simulation model and/or FOTs.

Currently the history-matched model is used to further investigate what areas have been swept by injection water (using streamlines) and also what potential remediation activities could

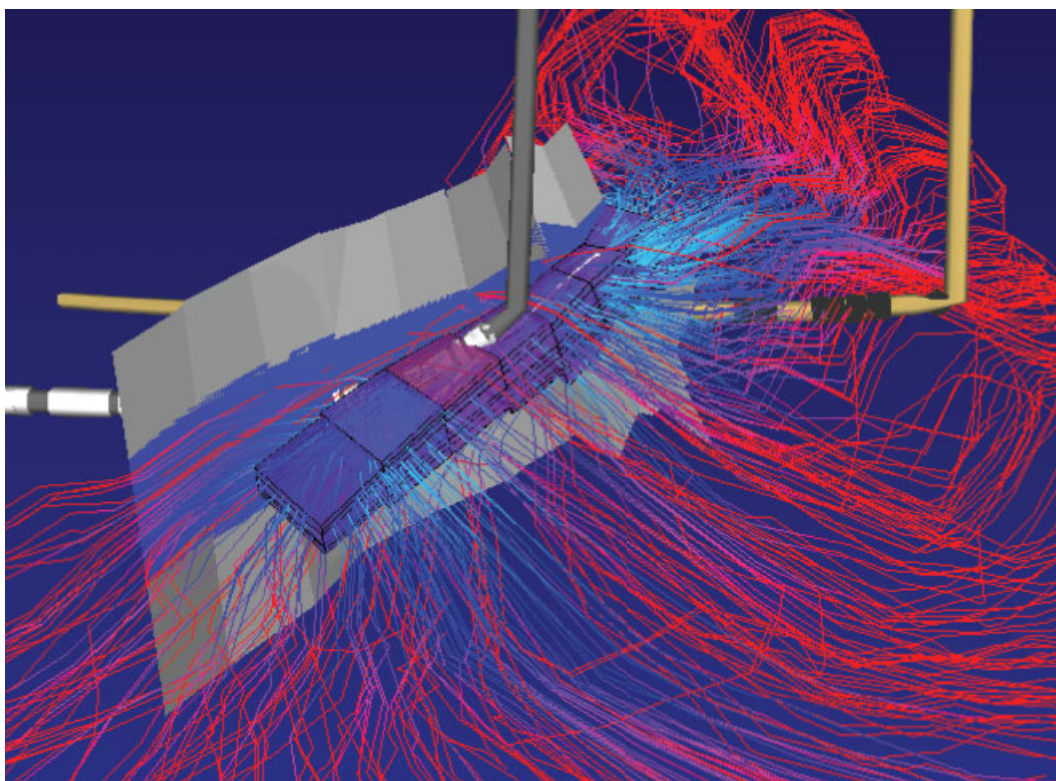


Fig. 17—Streamlines emerging from the induced fracture.

be executed to recover the remaining previously bypassed oil. An example of the streamlines coming out of the induced fracture at the end of the history-match simulation in June 2007 is shown in Fig. 17. Only the gridblocks that are connected by the induced fracture are plotted together with the streamlines colored with respect to time of flight.

Conclusions

We used injection/production and pressure data and fracture-simulation tools to investigate the response of one injector/producer pair in the Pierce waterflood. The results indicate a vertically contained fracture with half-length of 700–850 ft and height of 50–100 ft. The work demonstrates that a growing-fracture scenario is a very likely explanation for the fast water breakthrough at Producer A1 and confirms that dynamic fractures on the order of the well spacing under historical injection rates are a major concern for any water-injection strategy in Pierce. The FRAC-IT™ model(s) combined with the presented data analysis leads the way to actively handle the waterflooding issues. So far, the results of this study and similar investigations for the other Pierce injector/producer pairs have led to the following:

- Operating envelope: Maximum injection rates are set for injectors in order to keep expected fracture sizes well below the well distance and to give better areal sweep.
- THP surveillance: Dedicated FOTs are included as a formal part of the well and reservoir-surveillance plan.
- FRAC-IT: Sector models are incorporated in the full-field model. The model is used to decide on optimal water-injection rates (optimal sweep) at mid-long term, in combination with development options (infill drilling) and vs. alternative reservoir-management scenarios, such as lowering of the gas/oil contact.

Induced-fracture propagation is a major issue because fracture dimensions on the order of the well spacing can increase very quickly, thereby bypassing potentially unswept reservoir rock and shortcutting injectors and producers. For this reason, the method and conclusions presented in this paper, together with the results from similar work on the other water injectors in the field, are playing a key role in the short- and long-term waterflood optimization of the Pierce field.

Nomenclature

- A_p = poroelastic constant
 C = used in the ICSF model to describe the wellbore storage coefficient
 dS_3 = change in minimum horizontal stress
 DP = pressure difference
 FcD = used in the IFO model to describe the dimensionless fracture conductivity
 F_{skin} = used in the ICSF model to describe the fracture-face damage
 h = used in the ICSF model to describe the total injection-layer height
 hf = used in the ICSF model to describe the total fracture height (that is constant over time)
 $hf1$ = used in the IFO model to describe the fracture height upward measured from the fracture-initiation point (center of elliptical fracture)
 $hf2$ = used in the IFO model to describe the fracture height downward measured from fracture-initiation point (center of elliptical fracture)
 $hf1^{bf}$ = as $hf1$, but value for best match result
 $hf2^{bf}$ = as $hf2$, but value for best match result
 k = permeability
 kh = permeability-height product
 L = used in the ICSF and the IFO models to describe the distance from the fracture to the fault
 S_{kin} = used in the ICSF model to characterize any restrictions between the reservoir and the point of measurement
 X_f = used in the IFO and ICSF models to describe the fracture half-length measured from the fracture-initiation point (center of elliptical fracture). Note that the fracture is symmetric.

Acknowledgments

The authors are grateful to Shell International Exploration & Production, Shell Exploration & Production in Europe, Oranje-Nassau Energie B.V., and Nippon Oil Exploration & Production U.K. Limited for

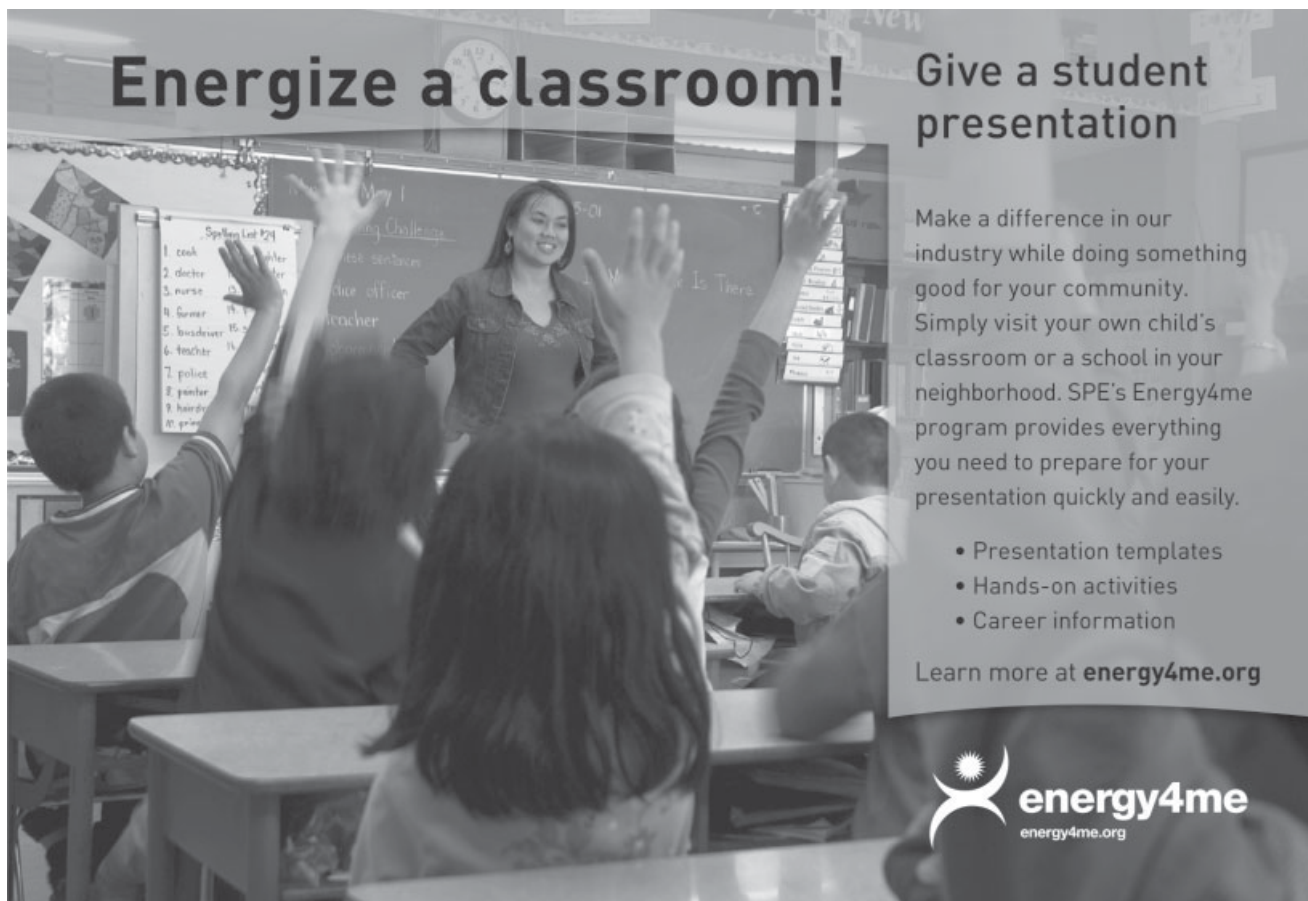
permission to publish this work. The authors would like to thank Arno van den Haak, Paul van den Hoek, Peter Schutjens, and the Pierce subsurface team members for support and technical discussions.

References

- Hustedt, B., Qiu, Y., Zwarts, D., and van den Hoek, P.J. 2005. Modeling Water-Injection Induced Fractures in Reservoir Simulation. Paper SPE 95726 presented at the SPE Annual Technical Conference and Exhibition, Dallas, 9–12 October. doi: 10.2118/95726-MS.
- Hustedt, B., Zwarts, D., Bjoerndal, H.-P., Masfry, R., and van den Hoek, P.J. 2008. Induced Fracturing in Reservoir Simulations: Application of a New Coupled Simulator to a Waterflooding Field Example. *SPE Res Eval & Eng* 11 (3): 569–576. SPE-102467-PA. doi: 10.2118/102467-PA.
- Tran, D., Settari, A., Nghiem, L. 2002. New Iterative Coupling Between a Reservoir Simulator and a Geomechanics Module. Paper SPE 78192 presented at the SPE/ISRM Rock Mechanics Conference, Irving, Texas, USA, 20–23 October. doi: 10.2118/78192-MS.
- van den Hoek, P.J. 2005. Dimensions and Degree of Containment of Waterflood-Induced Fractures From Pressure-Transient Analysis. *SPE Res Eval & Eng* 8 (5): 377–387. SPE-84289-PA. doi: 10.2118/84289-PA.
- van den Hoek, P.-J., Hustedt, B., Sobera, M., Masfry, R.A., Snippe, J., and Zwarts, D. 2008. Dynamic Induced Fractures in Waterfloods and EOR. Paper SPE 115204 presented at the SPE Russian Oil and Gas Technical Conference and Exhibition, Moscow, 28–30 October. doi: 10.2118/115204-MS.
- van den Hoek, P.J., Matsuura, T., de Kroon, M., and Gheissary, G. 1999. Simulation of Produced Water Reinjection Under Fracturing

Conditions. *SPE Prod & Fac* 14 (3): 166–176. SPE-57385-PA. doi: 10.2118/57385-PA.

Bernhard Hustedt is currently working as a reservoir engineer with Brunei Shell Petroleum. He holds a BSc degree from Hamburg U. (Germany, 1997), an MSc degree from Leeds U. (England, 1998), and a PhD degree from the U. of Nice-Sophia Antipolis (France, 2002), all in geophysics. Hustedt has been publishing technical work related to seismic wave attenuation, 3D seismic wave propagation modeling, and dynamic fracture propagation modeling using coupled fluid-flow and geomechanics simulators. In 2009, he received the Cedric K. Ferguson Medal (SPE) for outstanding contributions in petroleum engineering. **Jeroen Snippe** is a senior reservoir engineer with Shell. After obtaining a PhD degree in physics at Leiden U. (Netherlands, 1997) he joined the reservoir simulator development team at Shell International's research center in The Hague. In this role, Snippe's focus was on static-dynamic model integration, gridding and upscaling, as well as simulation modeling consultancy and training. In 2003 Jeroen moved to Shell U.K. in Aberdeen where he worked on several North Sea oil and gas fields (infill drilling and field redevelopment). Since 2007 he worked on the Pierce field with primary focus on well and reservoir management. In July 2009 he moved back to The Netherlands. After a short step-out to gas exploration (well planning and well testing) Snippe is specializing in advanced modeling techniques for CO₂ storage (coupled fluid-flow, PVT, and chemical reactions).




Energize a classroom!

Give a student presentation

Make a difference in our industry while doing something good for your community. Simply visit your own child's classroom or a school in your neighborhood. SPE's Energy4me program provides everything you need to prepare for your presentation quickly and easily.

- Presentation templates
- Hands-on activities
- Career information

Learn more at energy4me.org

 **energy4me**
energy4me.org